Electronic Supplementary Material (ESI) for Materials Horizons.

Supplementary Materials

Abnormal In-plane Epitaxy and Formation Mechanism of Vertically Aligned Au Nanopillars in Self-Assembled CeO_2-Au Metamaterial System

Juanjuan Lu[a], Di Zhang[a, b], Robynne L. Paldi[a], Zihao He[c], Ping Lu[d], Julia Deitz[d], Ahmad Ahmad[a], Hongyi Dou[a], Xuejing Wang[a], Juncheng Liu[a], Zedong Hu[a], Bo Yang[a], Xinghang Zhang[a], Anter A El-Azab[a], Haiyan Wang[a,c,*]

[a] School of Materials Engineering, Purdue University, West Lafayette, Indiana 47907, United States

[b] Center for Integrated Nanotechnologies (CINT), Los Alamos National Laboratory, Los Alamos, NM 87545, United States

[c] School of Electrical and Computer Engineering, Purdue University, West Lafayette, Indiana 47907, United States

[d] Sandia National Laboratories, Albuquerque, NM 87185, USA

[*]Corresponding author: hwang00@purdue.edu

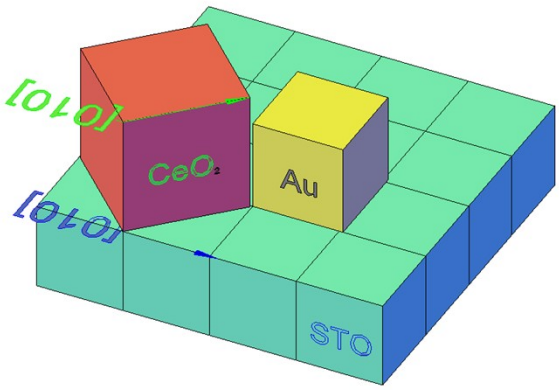

Fig. S1 Illustration of expected epitaxial relationships between CeO_2, Au and STO based on the strain compensation model.

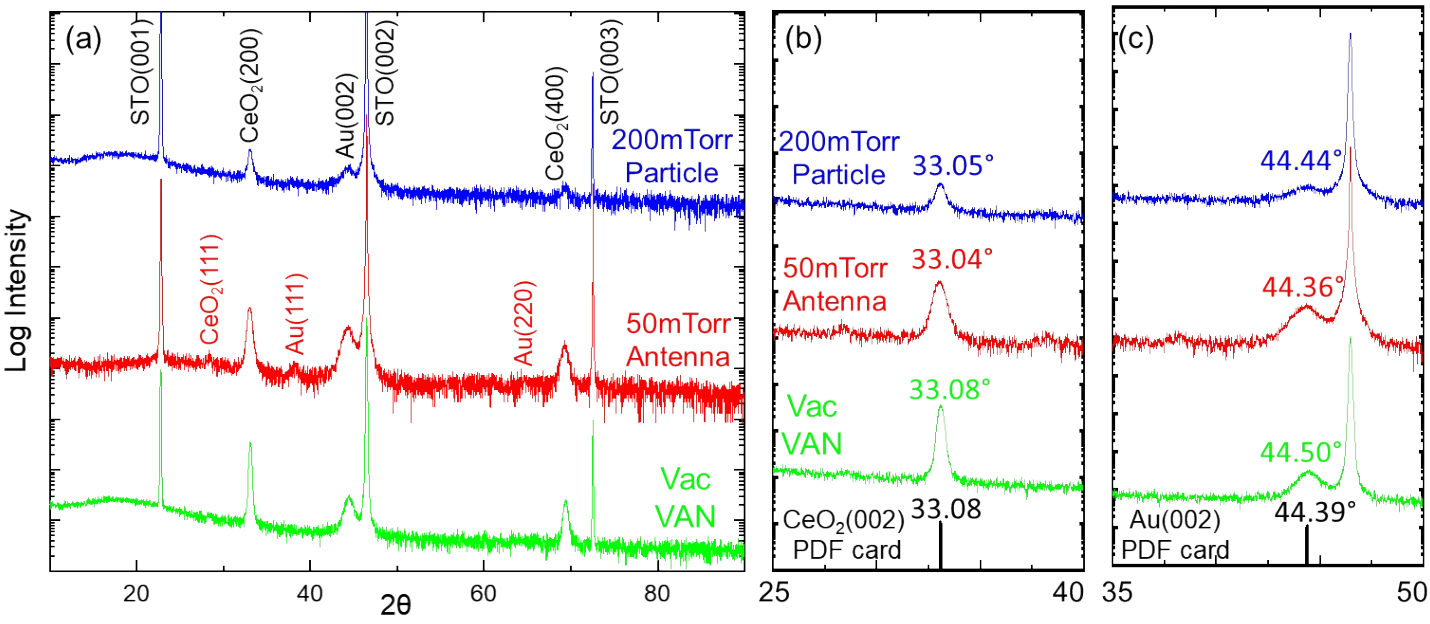

Fig. S2 XRD patterns of (a) CeO_2-Au films with particle, antenna and nanopillar Au morphologies; (b) and (c) enlarged 25°-40° and 35°-50° area of (a) showing the peak locations of CeO_2(002), Au(002) for the three sets of films and the standard PDF card. Compared to the bulk materials, minor changes in the peak positions of CeO_2-Au thin films demonstrate little or no strain from out-of-plane direction for CeO_2 and Au phases in these films.

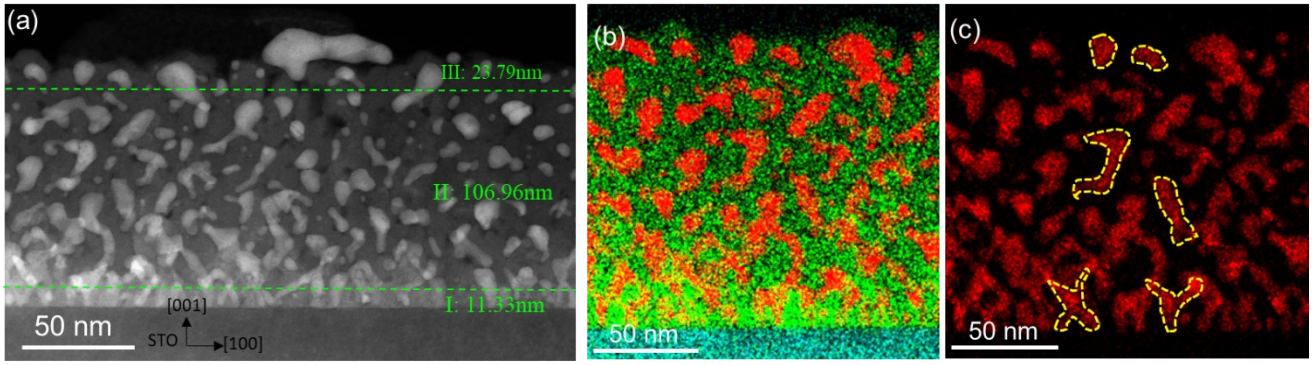

Fig. S3 Additional set of STEM and EDS images showing cross-sectional morphology of the thinner area in the nanoantenna sample. (a) is the overall STEM image and the dashed lines indicate the three growth sections in this film. (b) and (c) are EDS images with Au, Ce and Ti elements. (c) is EDS image showing only Au element. It should be noted that, because the right side of (a) is too thin, it was partly damaged by the ion milling process during the TEM sample preparation. Thus, the nanoparticle-in-matrix morphology on the right part cannot represent the morphology of this nanoantenna sample.

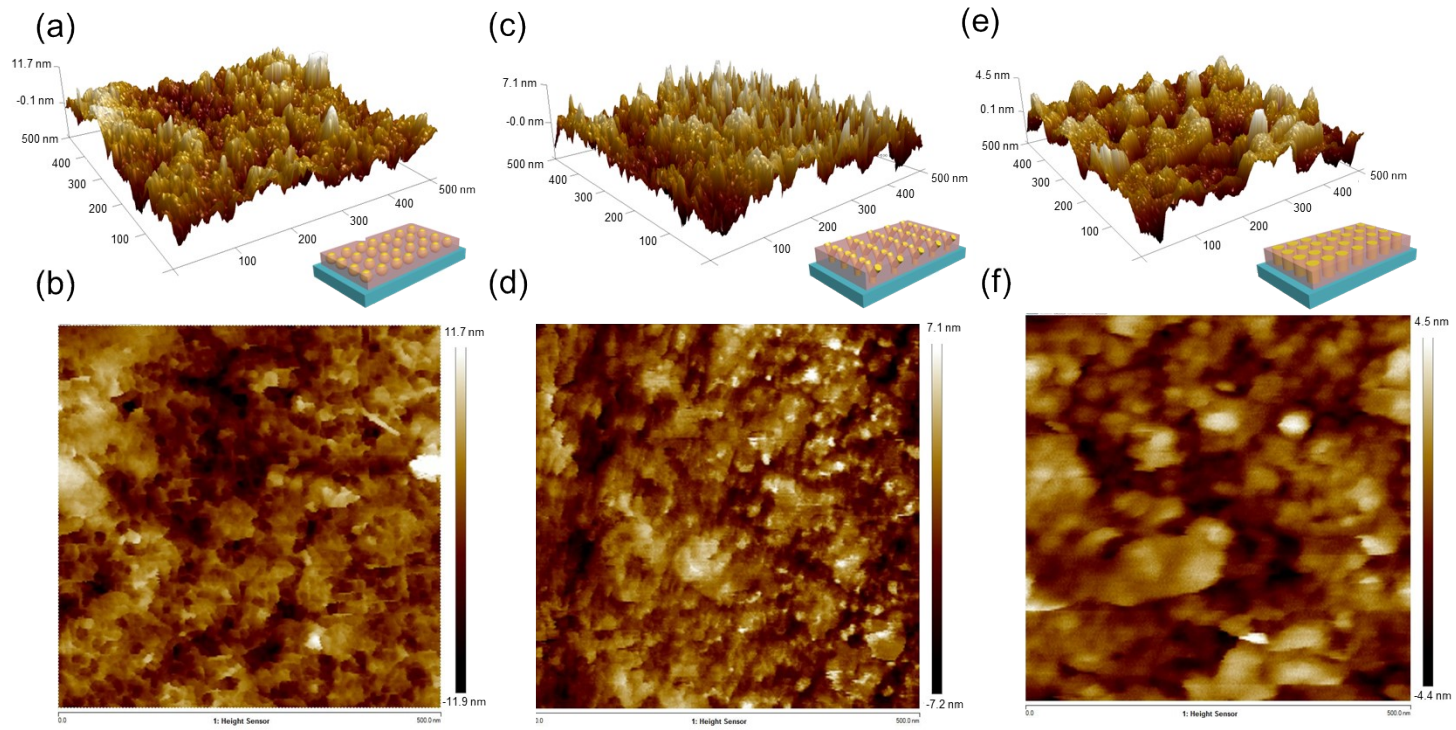

Fig. S4 3D and 2D surface roughness mappings for (a),(b): the CeO_2-Au PIM sample, (c) and (d): the nanoantenna-in-matrix sample, and (e) and (f): the VAN sample. The results are generated from AFM scan measurements of the thin film surfaces.

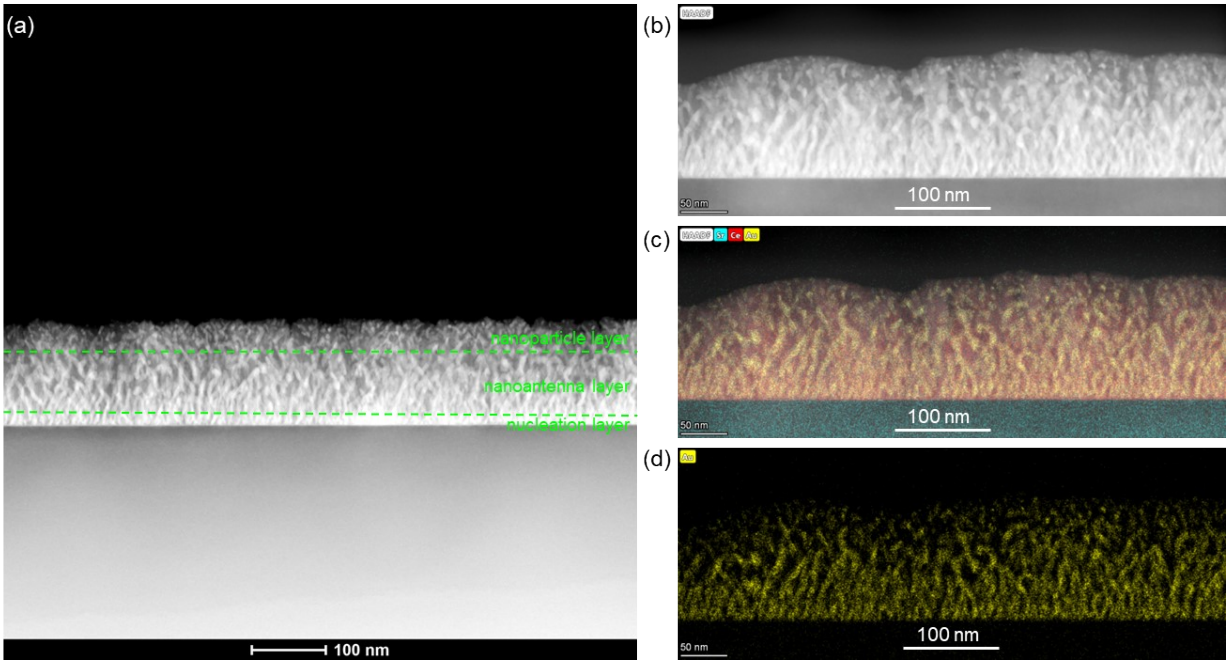

Fig. S5 (a) STEM, (b-d) EDS images of a CeO_2-Au nanocomposite film grown in 100mTorr oxygen background pressure. The morphology of this sample appear to be similar to that of the nanoantenna sample described in Figure 2(d-f), with three clear phase growth steps as divided in Figure S3(a). The separation between the second and top layer becoms less appearent in this sample. And the tilted angle α is smaller than the nanoantenna sample described in the paper, due to the change of connected tilted thin nanopillars into disconnected nanoparticles. Thus the top nanoparticle layer is considered comparatively thicker than Fig. 2 (d-e).

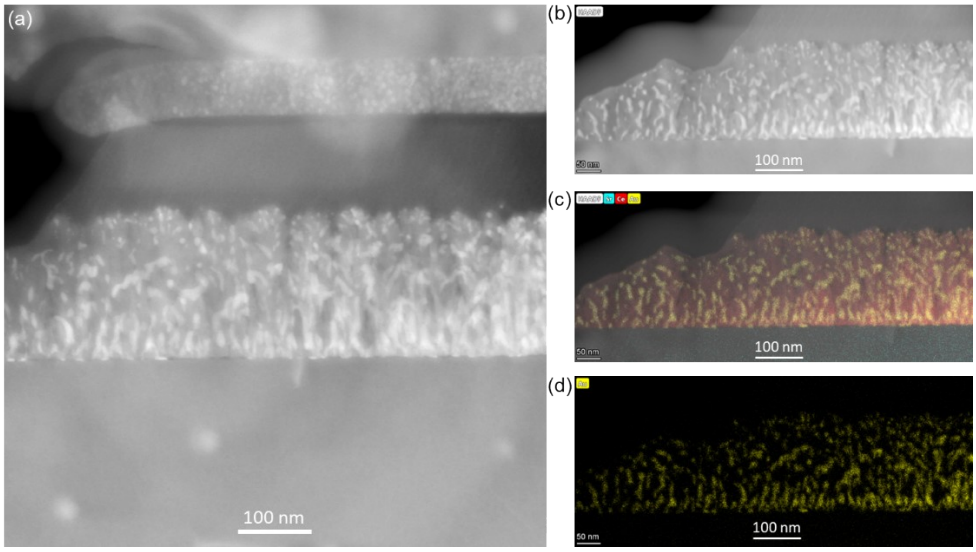

Fig. S6 (a) STEM, (b-d) EDS images of a CeO_2-Au nanocomposite film grown under 150mTorr oxygen background pressure. Compare this sample with the 100 mTorr sample in Figure S5, there is an obvious change of the Au nanoinclusion morphology to nanoparticles in this case. Most portion of the sample has turned into nanoparticle-in-matrix morphology compared to Fig. S5. But compare to the PIM sample shown in Fig. 2 (a-c), the PIM sample demonstrates more distictive and disconnected Au nanoparticles throughout the film thickness. Results from Fig. S5 and Fig. S6 are clear demonstrations for the gradual modulation of CeO_2-Au morphologies from nanoantenna to PIM, as described in the paper. They also verified the existence of the special nanoantenna aggregation morphology in the nanoantenna sample, distinctive from either PIM or VAN morphology.

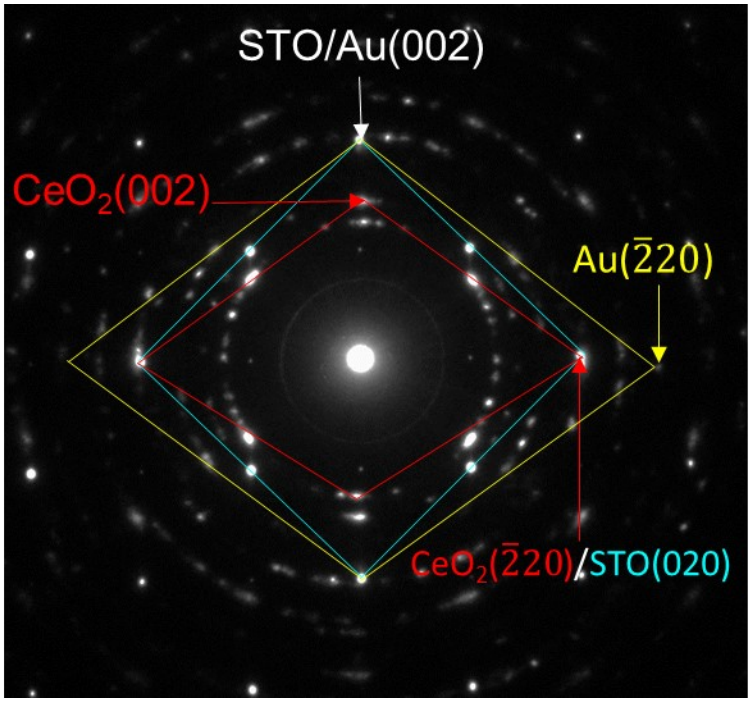

Fig. S7 The diffraction pattern for Figure 3(a) confirming the abnormal in-plane epitaxy of Au (110)// CeO_2(110)//STO(010).

Table S1 Lattice Misfit of Different IP epitaxy

Matching Planes(A//B)	Preferrable Lattice Matching (A:B)	Calculated Misfit (A to B) $(f = 2 \times \frac{a_A - a_B}{a_A + a_B})$
Au(110)//STO(001)	4:3 (Domain matching)	1.54
Au(001)//STO(001)	1:1 (Cube on cube)	-4.36%
CeO_2(110)//STO(001)	1:1 (Cube on cube, 45°Rotated)	2.05%
CeO_2(110)//Au(001)	1:1 (Cube on cube, 45°Rotated)	6.39%
CeO_2(110)//Au(110)	3:4 (Domain matching)	4.85%

The first column of this table gives the theoretically possible lattice matching combinations in this CeO_2-Au/STO thin film system. The second column describes the lattice matching types with minimum strain. And the third column is the calculated misfit values for the corresponding matching types. The green color-coded matching plane combinations are the ones experimentally adopted in this CeO_2-Au/STO thin film system.

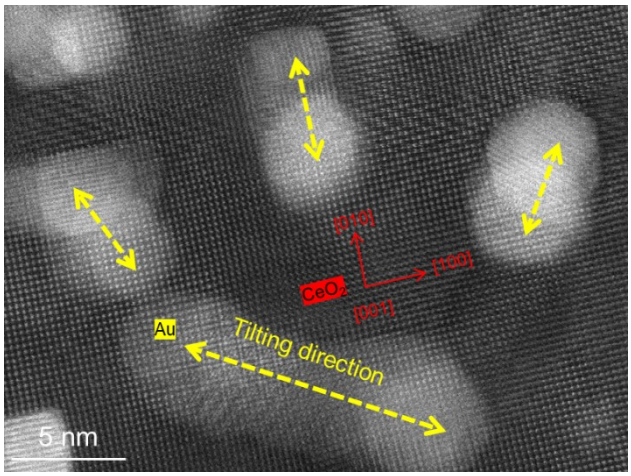

Fig. S8 The random tilting directions for circular shaped pillars.

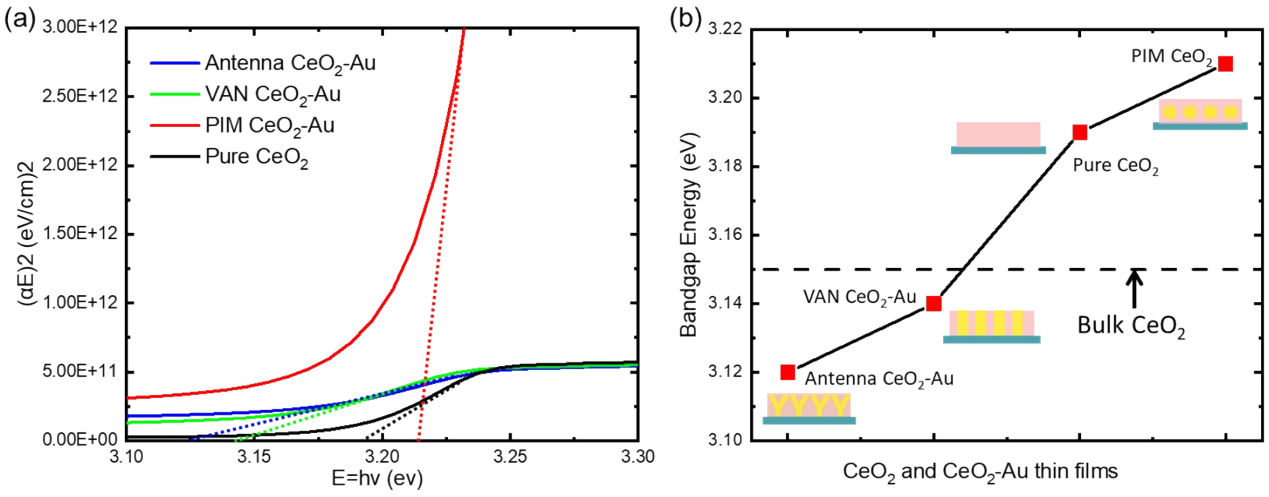

Fig. S9 The bandgap calculations. (a) is the *hv* - $[(\alpha hv)]^2$ curve with the extrapolation showing the bandgaps of each sample. (b) shows the relationships of bandgap and the morphologies in CeO_2-Au/STO thin films.

The addition of Au into CeO_2 results in bandgap tuning in this nanocomposite system. According to the solid band theory, bandgaps of all four samples are calculated from the optical transmittance data and based on the following Equation 1.1:

$$(\alpha hv)^n = \beta(hv - E_g) \qquad (1.1)$$

Where n=2 for direct band gap and n=1/2 for indirect band gap. α and β are absorption coefficient and tailing factor, which are constants. E_g represents the bandgap energy and hv is the energy of the incident light. In this case, the bandgap values are retrieved by the extrapolation of the hv-$(\alpha hv)^n$ curve. It is known that bulk STO has the bandgap of 3.25eV[1], and the bandgap of bulk CeO_2 is 3.15eV[2]. The addition of Au into the CeO_2 thin film demonstrates a minor tuning in the bandgap values. As shown in Figure S7 (a), the bandgaps for pure CeO_2, PIM, VAN and nanoantenna samples are 3.19eV, 3.21eV, 3.14eV and 3.12eV.

The nanoantenna, VAN samples have analogous values while the PIM sample has the largest bandgap, similar to that of the pure CeO_2 film. The tuning of bandgaps is shown by the graph in Figure S 7(b), with the dashed line representing the reported bulk CeO_2 bandgap of 3.15eV. Overall, the band gaps of the films tend to decrease slightly, indicative of an increase in the free electron carrier density. While the thickness of these CeO_2-Au films is increasing, [3] the more intricated Au morphology reduces the thin film bandgap.

[1] T. K. Townsend, N. D. Browning, F. E. Osterloh, *ACS Nano* **2012**, *6*, 7420.

[2] Z. Wang, Z. Quan, J. Lin, *Inorg Chem* **2007**, *46*, 5237.

[3] S. Debnath, M. R. Islam, S. R. Khan, *Bull. Mater. Sci* **2007**, *30*, 315.

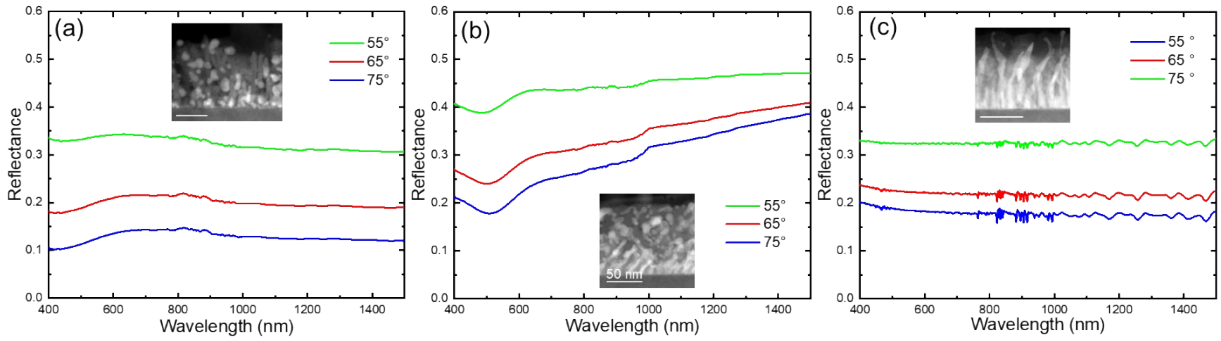

Fig. S10 The angular dependence of reflectance for PIM, antenna and VAN samples

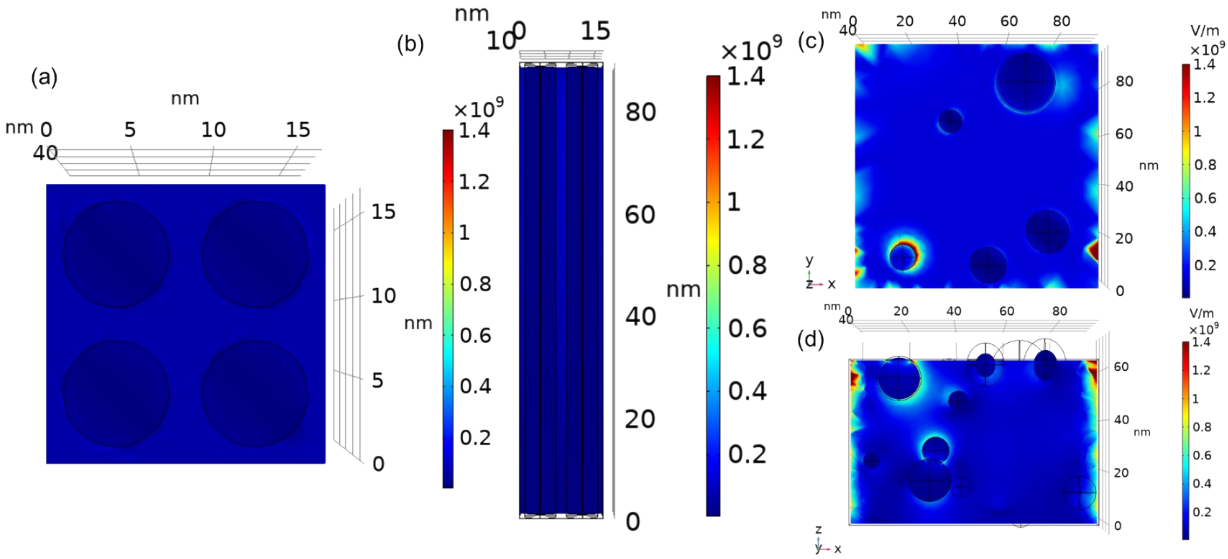

Fig. S11 The EFM profiles of CeO_2-Au VAN sample obtained from (a) XY plane and (b) YZ plane under 1500 nm illumination. (c) and (d) are the XY plane EFM profiles and YZ plane EFM profiles for PIM sample under 1500 nm illumination.

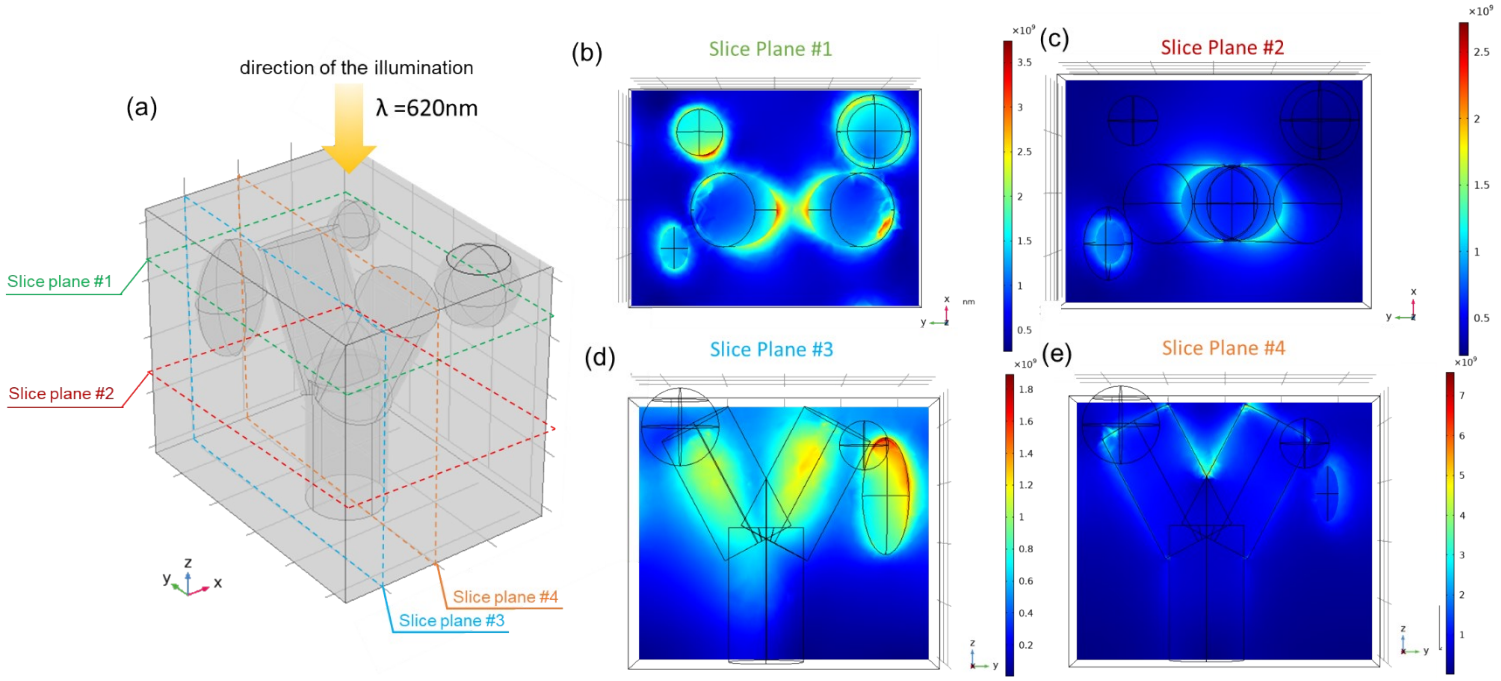

Fig. S12 EFM profiles for the illustration of the nanoantenna CeO_2-Au sample at incident light wavelength = 620nm. (a) The illustration geometrical model. The model is composed of a nanoantenna structure unit at the center and a thin PIM layer at the top. (b) and (c) the XY plane EFM amplitude profiles for (a) at different z coordinated as illustrated in the green and red colors. (d) and (e) are the YZ plane sliced EFM at different x coordinates as coded by the blue and orange colors. Comparing (b), (d) with (c) and (f), it is found that at locations where nanoinclusions are located more adjacent to each other, the electric field enhancement is more obvious.

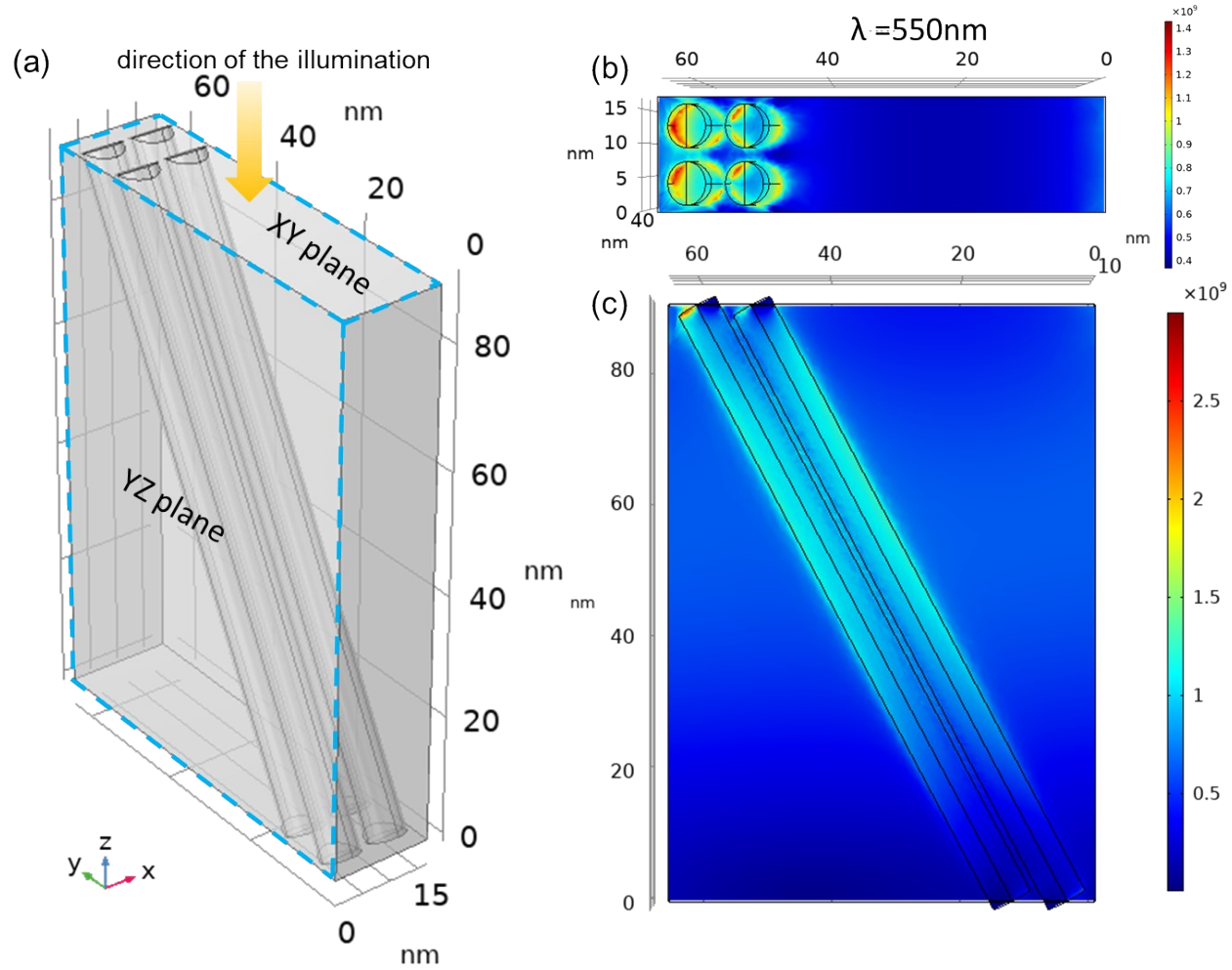

Fig. S13 The geometrical model of a tilted VAN with α = 62° and the corresponding EFM amplitude profiles. (a) the geometrical model of the tilted VAN with a tilting angle α = 62°. All other parameterers are the same with the VAN sample. (b) is the XY plane EFM amplitude profile of (a) under an incident illumination of λ= 560nm. (c) is the YZ plane EFM amplitude profile of (a) at the center of the pillars under an incident illumination of λ= 560nm. Note that the scale bar is set to be one magnitude higher than in Figure 5(d).

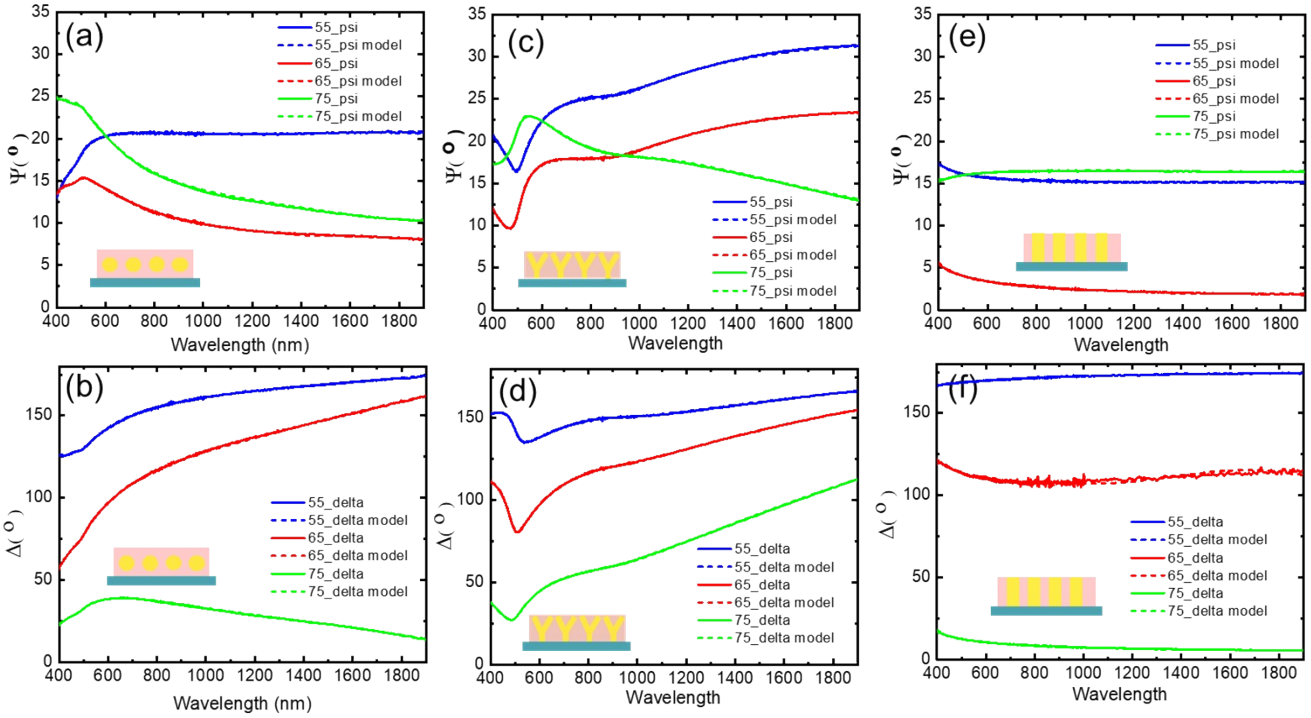

Fig. S14 Original psi and delta data of (a) and (b) the PIM CeO_2-Au sample, (c) and (d) the antenna sample, and (e) and (f) the VAN sample. Spectroscopic ellipsometry (SE) measurements is a technique that evaluates the polarization variance of the reflected light from the sample surface. Herein, the refractive index and dielectric functions, as well as anisotropy, can be derived. From the SE measurement, psi (ψ) and delta (Δ) data, which are representatives of the changes of the amplitude ratio and phase difference of the optical wave polarization, were firstly obtained and fitted to derive the dielectric functions from IP and OP directions.

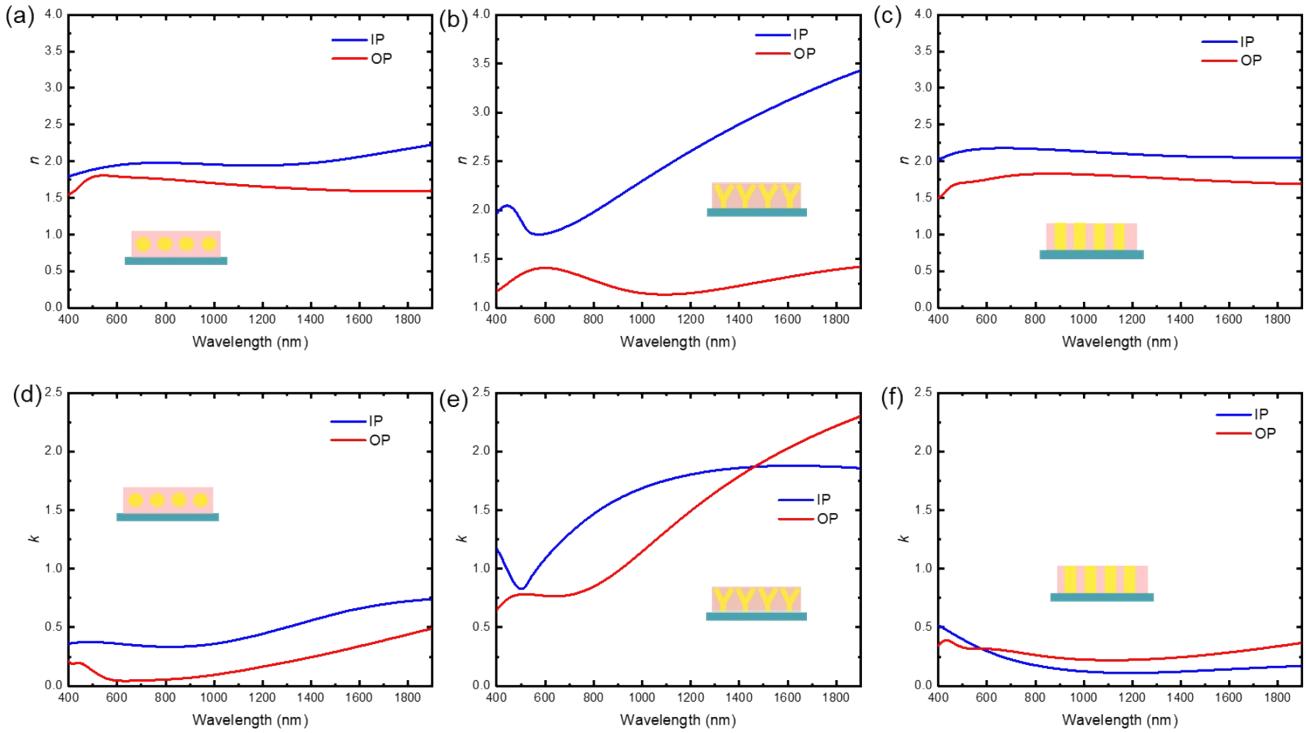

Fig. S15 The n (extinction coefficient) and k (the index of refraction) spectra simulated from the ellipsometry measurement for: (a) and (d) the PIM CeO_2-Au sample, (b) and (e) the nanoantenna sample, (c) and (f) the VAN sample. The inset illustrations are the corresponding cross-sectional morphologies of each sample. From the figure, the extinction coefficient appears to be the largest in the nanoantenna sample compared to the other two samples, similar to the imaginary permittivity data. This confirms the conclusions made regarding the strongest LSRP responses in the nanoantenna sample. Also, the peak locations in each extinction coefficient spectrum is slightly shifted from the LSPR locations decided by the transmittance and reflectance data. This is because the simulations were conducted considering the sample a uniaxial model, giving two individual graphs from IP and OP directions. The LSPR locations determined upon the extinction coefficient spectra corresponds with the assumptions made in section 2.2.1.